PERGAMON

International Journal of Heat and Mass Transfer 43 (2000) 3579–3588

International Journal of HEAT and MASS TRANSFER

www.elsevier.com/locate/ijhmt

Fouling in enhanced tubes using cooling tower water Part II: combined particulate and precipitation fouling

Wei Li[a], Ralph L. Webb[b,*]

[a]*Engineered Air, 320580 W. 83rd Street, DeSoto, KS, USA*
[b]*Department of Mechanical Engineering, Pennsylvania State University, University Park, PA 16802, USA*

Received 5 February 1999; received in revised form 10 December 1999

Abstract

This work addresses fouling in a family of seven internally helically ridged tubes, which have different ridge heights, helix angles, and a number of ridge starts. Of specific interest are long term, combined precipitation and particulate fouling (P&PF) in cooling tower systems, and accelerated particulate fouling. The comparison of the P&PF and accelerated particulate fouling data shows a unique relationship. This allows one to infer the relative long-term P&PF performance of different enhanced tube geometries from accelerated particulate fouling data. For a small number of ridge starts (less than 25) and helix angles below 35°, the fouling resistance is proportional to the heat transfer coefficient (or the mass transfer coefficient, via the heat–mass transfer analogy). However, for a large number of starts and high helix angles (e.g., 45°), the fouling factor is considerably higher than one would predict, based on the mass transfer coefficient. It appears that this occurs because of low shear stress (affecting the foulant removal rate) in the interfin region. Recommendations are offered on geometries that will avoid high fouling penalty.

1. Introduction

The combination of long-term precipitation fouling and particulate fouling (P&PF) in condensers using cooling towers was reported in Part I by Webb and Li [1]. In the present work (Part II), we will define a relationship between long term P&PF and accelerated particulate fouling.

Fouling is a slow process. It may take months to build up in actual situations. Little work has been done on *long term* fouling in enhanced tubes. Rabas et al. [2] monitored the fouling characteristics of helically corrugated steam condenser tubes in an electric utility plant for 15 months. This condenser used the Wolverine Korodense corrugated tube with river water operating at 1.25–2.75 m/s water velocity. They found that the fouling rates of the enhanced tubes ranged from about the same as, to about twice that of, the plain tubes.

Most investigators have performed accelerated particulate fouling tests. Kim and Webb [3] performed accelerated particulate fouling tests of three repeated rib tubes ($0.015 \le e/D_i \le 0.030$ and $10 \le p/e \le 20$) and a smooth tube for $14{,}000 \le Re \le 26{,}000$ using ferric oxide and aluminum oxide particles. They found that the fouling resistance of the repeated rib tubes was higher than those of smooth tubes at low *Re*. However, at high

* Corresponding author. Tel.: +1-814-865-0283, fax: +1-814-865-1344.

E-mail addresses: weili@idir.net (W. Li), rlwebb@psu.edu (R.L. Webb).

0017-9310/00/$ - see front matter
PII: S0017-9310(99)00393-2

Nomenclature

$A_{i,\,nom}$	nominal internal surface area based on plain tube ($A_{i,\,nom} = \pi D_i L$) (m^2)
B	time constant in Kern–Seaton (1959) model (s^{-1})
c_p	specific heat at constant pressure (J/kg K)
D_i	internal tube diameter to the base of enhancement (m)
e	surface roughness height (m)
h	heat transfer coefficient based on $A_{i,\,nom}$ (W/m^2 K)
K_m	mass transfer coefficient based on $A_{i,\,nom}$ (kg/m^2 s)
L	tube length (m)
Pr	Prandlt number
p	axial pitch of the rib (m)
R_f	fouling resistance based on $A_{i,\,nom}$ (m^2 K/W)
R_f^*	asymptotic fouling factor (m^2 K/W)
$(dR_f/dt)_{t=0}$	initial fouling rate ($= BR_f^*$) (m^2 K/J)
R_0	fouling resistance of crystalline layer (m^2 K/W)
R_{total}	total fouling resistance of crystalline layer and P&PF layer (m^2 K/W)
Re	Reynolds number
Sc	Schmidt number
t	time (s)
U_c	overall heat transfer coefficient at clean tube conditions (W/m^2 K)
U_f	overall heat transfer coefficient at fouled tube conditions (W/m^2 K)
u_m	average fluid velocity in the tube (m/s)

Greek symbols

α	helix angle
ρ	fluid density (kg/m^3)
φ_d	rate of deposition (m^2 K/W s)
φ_r	rate of removal (m^2 K/W s)
τ_w	surface shear stress (N/m^2)

Subscripts

P&PF	combination of particulate fouling and precipitation fouling
p	plain surface
part	particulate fouling

Re (26,000), the fouling resistance was approximately the same as for the smooth tube value. The fouling resistance increases as e/D_i decreases and p/e increases. They developed the first accelerated particulate fouling model for enhanced tubes, which accounts for the effect of enhancement geometry on the fouling rate. Based on the heat-mass transfer analogy, they show that the mass transfer coefficient, which is proportional to the deposition rate, is proportional to the heat transfer coefficient.

Chamra and Webb [4] tested accelerated particulate fouling behavior for a wide range of particle size distribution and foulant concentration for two different types of in-tube enhancements and a smooth tube. They found that the fouling resistance of enhanced tubes are always higher than that of smooth tubes. They proposed that their correlation of fouling resistance as a function of foulant concentration and particle size, should be applicable to predicting long-term fouling resistance for actual river water. However, the in-plant data were not available for validation.

Somerscales et al. [5] compared the fouling characteristics of five different in-tube enhancements using accelerated particulate fouling. Contrary to Rabas et al. [2], Kim and Webb [3], and Chamra and Webb [4], their results suggest that the surfaces with a high clean tube heat transfer coefficient may have a lower fouling tendency than surfaces with a lower clean coefficient of heat transfer. Thus, they concluded that the corrugated and axial fin geometries are less susceptible to fouling than smooth tube. Somerscales et al. [5] proposed that one possible reason for the contrary results from the Rabas et al. [2] results is that several fouling mechanisms exist in the in-plant tests (e.g., precipitation and particulate fouling).

Investigators using accelerated tests have studied each mode separately. However, several investigators have proposed that an industrial fouling process may involve two or more fouling mechanisms simultaneously. Further study is required to explain the apparent differences between accelerated and in-plant results. One approach is to make both accelerated and long-term fouling tests on the same tube and compare the results. This is the objective of the present study.

2. Particulate fouling versus P&PF

In the past 20 years, several investigators noticed the phenomenon that precipitation fouling occurs in conjunction with particulate fouling. Taborek et al. [6] and Epstein [7] emphasized that combined particulate fouling and precipitation fouling at relatively low tem-

peratures may loosen the bond strength of the crystalline structure. Cooling tower water contains a high concentration of a variety of salts, each exhibiting different crystalline formations. Consequently, crystalline clusters build up in irregular patterns, forming cavities between them which permit deposition of suspended particles, further decreasing the crystalline cohesion.

Yiantsios et al. [8] proposed that the presence of suspended particles may affect the rate of crystallization fouling and may drastically modify the compactness, the physical properties and even the morphology of the deposits. In industrial situations, a considerable part of the particulate matter is of colloidal dimensions, which may pass through a filter. These colloidal particles may be indigenous (through bulk precipitation and silica polymerization, or from the removal of deposits) or they can enter the process streams with the make-up water. The particulate deposits consist of flocculates of small needle-like particles, while the combined deposits consist of calcite and aragonite particles and of the added particulates. They thought that the increased mass of deposits collected in the combined runs is not due to particulate deposition, but rather to an enhanced wall crystallization rate induced by the presence of the particulates. They stated that there is no explanation for the observed synergistic effect of particulates on the combined deposition rates.

Hasson [9] proposed a possible mechanism to explain the increase in deposit porosity with increasing particle concentration. He proposed that, at any given time, the crystallizing deposit surface is partly covered by particles that have been transported to the wall by diffusion. Adherence of the particles is weak. During the residence time of a particle on the deposit, crystal growth occurs on the particle and hence the area occupied by the particle will not have experienced growth relative to the neighboring, particle-free areas. This random coverage of the deposit, by temporarily residing particles, promotes deposit porosity and acts to decrease deposit mass growth rates. He anticipated that an increase in particle concentration will increase the occupied surface and hence the porosity of the deposit, while an increase in velocity will have the opposite effect.

Bansal et al. [10] investigated the effect of crystallizing and non-crystallizing particles on fouling of calcium sulfate in a plate heat exchanger. There used two types of suspended particles in the water that caused particulate fouling: (1) Non-crystallizing particles, and (2) Entrained crystallizing particles. Calcium sulfate particles (crystallizing particles) are formed during the preparation of calcium sulfate solution and are due to breakage of calcium sulfate crystals growing on the heat transfer surface. These suspended particles settle on the heat transfer surface and act as nuclei. The availability of extra nucleation sites increases the crystallization rate significantly. Alumina particles (non-crystallizing particles) were purposely added during the preparation of calcium sulfate solutions. These particles attach loosely to the heat transfer surface compared with crystalline deposits, which adhere strongly. Therefore, calcium sulfate crystals growing on these particles are removed easily. Also alumina particles settling on the growth faces of calcium sulfate may act as a distorting agent. This slows the growth of the crystals. They found that the deposits attach loosely to the heat transfer surface. Therefore, calcium sulfate crystals growing on these particles are removed easily.

Rust and dust particles are commonly contained in cooling tower waters. Based on the above studies, it is probable that both precipitation and particulate fouling will occur. The effect of the non-crystallizing particles will be to decrease the bond strength and decrease the shear resistance of the structure. Following the long-term test reported by Webb and Li [1], they removed the tubes and made cross-section photos of the fouled tubes (Fig. 12 in Webb and Li [1]). They observed that the deposit was relatively "fluffy" and could be easily removed by brushing. The loose deposit structure shows that both particulate and precipitation fouling existed, and suggests that particulate fouling may be the dominant mechanism. The removed foulant samples were also chemically analyzed with the results given in Table 1. The analysis showed the following composition:

1. 57% is calcium carbonate.
2. 2% is calcium phosphate.
3. 14% non-carbonate "loss on ignition" determined by combustion of the foulant residue. This is either organic material or water content.
4. 26% particulates, which consist of 9% silica (from sand particles in water), 5% copper oxide (from copper tubing), 9% iron phosphate/silicate (from iron piping), and 3% aluminum silicate (from unidentified aluminum in the system).

The 59% calcium deposits are caused by precipitation fouling. The remaining 40% is from non-crystallizing particles, which should be due to particulate fouling. This observation suggests that both precipitation and particulate fouling occurred, as observed by Bansal [10]. We propose that after the induction period, precipitation fouling conditions are established. The cooling tower water also contains particulates in the form of dirt or rust at relatively low concentration (e.g., 50–100 ppm). These particulates are transported to the surface, where they are deposited among the precipitated particles. This combined fouling deposit exists as a soft and "fluffy" deposit, rather than the hard scale that is characteristic of pure precipitation fouling.

It may be possible to establish a relationship

between accelerated particulate fouling and the long-term P&PF in that occurs in the cooling tower system. If such a relationship can be established, it should be possible to predict the relative fouling tendencies of different enhanced geometries in cooling tower systems from the accelerated particulate fouling tests. This is the principal objective of the present study.

3. Proposed concept

Fouling is a rate-dependent phenomenon. The net fouling rate is the difference between the solid deposition rate and the removal rate. Kern and Seaton [11] proposed an asymptotic fouling model that is applicable to particulate fouling. They expressed the net fouling rate as the difference between the deposition and the removal rate:

$$\frac{dR_f}{dt} = \varphi_d - \varphi_r \tag{1}$$

They assumed the deposit accumulation was the result of two simultaneous opposing events, a constant deposition rate, φ_d and an increasing removal rate, φ_r. The φ_r is directly proportional to the mass of the fouling deposit per unit area. In principle, the model can embrace different fouling mechanisms providing the fouling is asymptotic. Both particulate fouling and precipitation fouling are due to the two competing processes. That means we can use Kern and Seaton's model [11] to analyze particulate fouling and P&PF, respectively. One may solve Eq. (1) to obtain:

$$R_f = R_f^*(1 - e^{-Bt}) \tag{2}$$

We propose that this model may be applied to particulate dominated P&PF. The proposed model is developed as follows:

$$R_f)_{total} = R_f)_0 + R_f)_{P\&PF} \tag{3}$$

The P&PF deposit is proposed to consist of two layers — a crystalline layer, $R_f)_0$, and P&PF layer, $R_f)_{P\&PF}$. At the beginning of deposit formation, the precipitation salt will have a well defined crystalline growth at the tube surface, which will depend on the wall temperature. The fouling resistance (R_0) should be a constant value during the formation of the asymptotic fouling resistance. The $R_f)_{P\&PF}$ is the fouling resistance of the layer which is just above the crystalline layer. This layer is the combination of particulate fouling and precipitation fouling (P&PF). Particulate fouling is assumed to dominate the P&PF layer. The deposits attach loosely compared with the crystalline layer.

However, only the P&PF layer exists in present study. Fig. 1 shows fouled and unfouled samples of Tube 2. Fig. 1(a) shows the original clean tube and Fig. 1(b) shows the fouled tube. We used a soft brush (a) to carefully clean sample, and (b) to obtain the foulant sample. During the cleaning process, we made sure that we removed only the loosely packed material (P&PF layer). Fig. 1(c) shows the Fig. 1(b) tube after this cleaning. By comparing Fig. 1(a) and (c), we can see that a crystalline layer does not exist. This is because the fouling surface temperature in this study is too low (below 90 F) to form a crystalline layer by inverse solubility salts. Therefore, $R_f)_0 = 0$ and the fouling resistance in the condenser tube of the cooling tower system is

$$R_f)_{total} = R_f)_{P\&PF} = R_f^*)_{P\&PF}(1 - e^{-Bt}) \tag{4}$$

4. Experimental program

Both accelerated and long-term fouling tests were taken in support of this work. The same tube geometries were tested in two totally different test facilities. In both the long term and the accelerated fouling tests, the R_f values are based on the nominal tube area

Table 1
Chemical analysis of fouling deposit by Diversey on 15 May 1995

Elemental analysis	Most probable composition
32% CO_3	32% Carbonate
22% Ca	57% Calcium carbonate, 2% calcium phosphate
14% NCLOI	14% Non-carbonate LOI
5% Si	9% Silica
4% Cu	5% Copper oxide
3% Fe	6% Iron phosphate, 3% iron silicate
1% Al	3% Aluminum silicate
1% P	Phosphorus
	Total 99%

defined as $A_{i,\,nom} = \pi D_i L$, where D_i is the tube diameter to the base of the enhancement. The uncertainty of the P&PF data is $\pm 6.2\%$, and the uncertainty of particulate fouling data is $\pm 11.8\%$. The facilities used and the experimental methods are described below.

4.1. Long term fouling tests

Part I of Webb and Li [1] reports cooling tower fouling data for the seven tubes having helical rib roughness geometries. The apparatus and experimental method are explained in the Part I paper. Both Rabas et al. [2] and Taborek et al. [6] showed that fouling for cooling of condenser cooling tower water has asymptotic behavior. Due to the test period time limitation (one cooling season), two of the enhanced tubes did not show fully developed asymptotic curves. The present use of curve-fitting of the data points, as shown in Fig. 3, is believed to be a viable method to determine the asymptotic value.

4.2. Accelerated fouling tests

Accelerated particulate fouling tests were also conducted using 3.0 μm aluminum oxide particles. The particulate fouling data were taken on Tubes 2, 3, 4, 5, and 8 (see Fig. 1 of Webb and Li [1]), and a plain tube. A series of tests at different concentrations and velocities was conducted by Li [13], who found that the particulate deposition rate increased with increasing Reynolds numbers. The data series for 1300 ppm foulant concentration at 1.07 m/s water velocity (Re = 16,000) is presented in this paper.

Since the apparatus and test procedure are fully described by Kim and Webb [3], only brief description will be given here. The apparatus has four fouling test sections, with one being a plain tube. Heat is transferred to the 3.05 m long test sections by condensing R-114 on the annulus side of the test section. Condensed R-114 is returned to the electric-heated boilers. Each test section has its own boiler, in which R-114 is heated by three electric band heaters (each of 1200 W capacity). Power to the band heaters is controlled by individual auto-transformers and the heat is removed from the test water in a plate heat exchanger. The fouling resistance is obtained by taking the difference between the overall thermal resistances for the fouled condition ($1/U_f$) and the clean tube condition ($1/U_c$). The data for U_f and U_c are taken at the same velocity, heat flux and water inlet temperature. The clean tube data were taken using clean water.

The apparatus was run for 2 h with clean water to reach a steady state. After it reached a steady state, the amount of particulate required for the desired ppm concentration was added to the system. This was taken as time zero for the fouling test. Asymptotic fouling

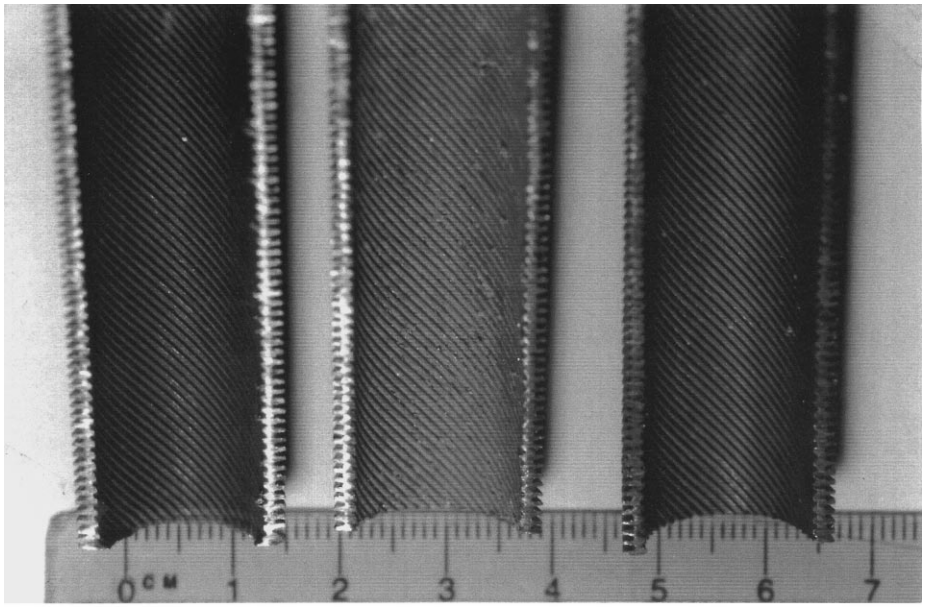

Fig. 1. Cross-section photos of Tube 2.

occurred in approximately 18 h. After the foulant was added, no additional foulant was added during the test period. This was done to prevent instabilities that could affect the fouling rate, or the retention of the foulant deposit. For a test started at 1400 ppm concentration, the foulant concentration decreased approximately 200 ppm during the test, yielding an average value of 1300 ppm during the fouling period. Repeat tests were also performed at the same particulate concentration (1300 ppm) and Reynolds number (16,000).

5. Experimental results

The tests results for the long-term P&PF cooling tower water fouling data are shown in Webb and Li [1]. Fig. 2(a) shows the accelerated particulate fouling curves for 1300 ppm concentration at 16,000 Reynolds number. This figure shows that the enhanced tubes exhibit higher fouling resistance than the plain tube. In addition, the fouling rate attains an asymptotic value in all the tubes. The greatest fouling increase occurred in Tubes 2, 3, and 5. These tubes also experienced significant long-term P&PF. The repeat accelerated particulate fouling test series is shown in Fig. 2(b).

Both the long-term P&PF and the accelerated particulate fouling data taken at $Re = 16{,}000$ were curve-fitted to the asymptotic Eq. (2). These curve fits provided the asymptotic fouling resistance (R_f^*) used for analysis of the fouling results. Fig. 3 shows a sample of curve-fit of the P&PF data of Tube 3. Table 2 gives the R_f^* values for the accelerated and P&PF fouling data. The tubes are ordered in the table (left to right) in order of decreasing R_f^*.

6. Discussion

6.1. Particulate fouling and P&PF relationship

Table 2 also shows the ratio of the R_f^* for the P&PF and particulate fouling data for each tube $[R_f^*)_{P\&PF}/R_f^*)_{part}]$. Examination of Table 2 shows that the $R_f^*)_{P\&PF}/R_f^*)_{part}$ ratio for all tubes is approximately equal ($4.57 \pm 14\%$). The initial fouling rate $(dR_f/dt)_{t=0} = BR_f^*$ ratio (P&PF-to-particulate fouling) also showed an approximately equal value for all tubes ($158 \pm 18\%$).

Using R_f^* values from Tables 2 and 3 shows the enhanced-to-plain tube R_f^* ratio for both the long term

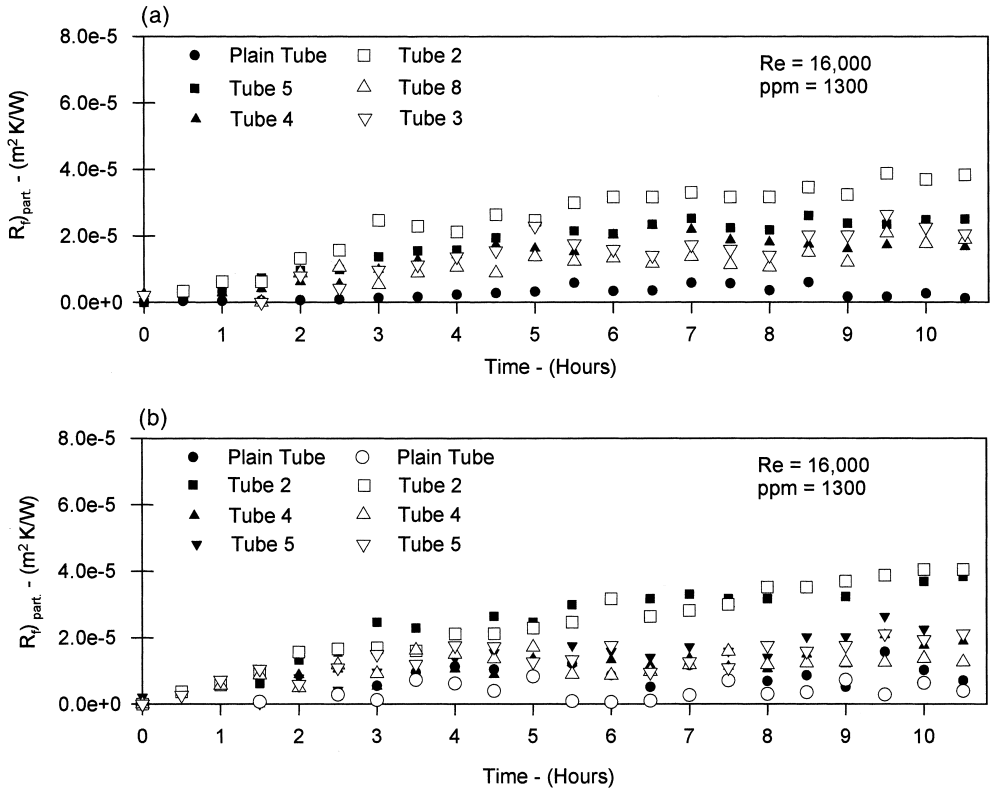

Fig. 2. (a) Repeatability of accelerated particulate fouling data, (b) accelerated particulate fouling data.

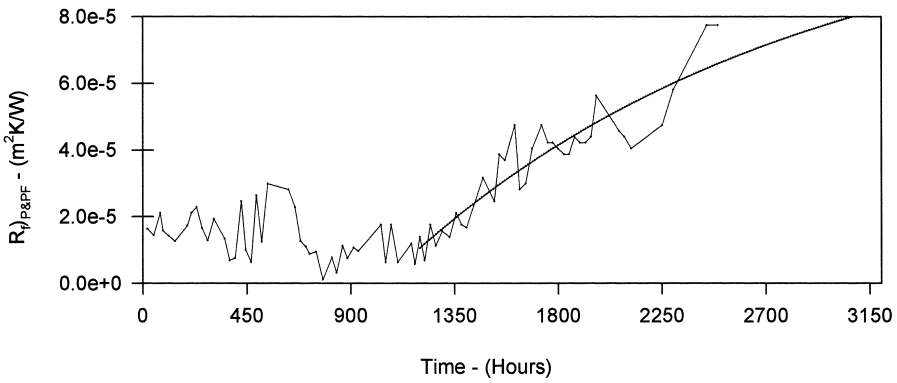

Fig. 3. Curve-fit of Tube 3 P&PF data.

P&PF and the accelerated particulate fouling. These are the ratios $R_f^*/R_{f,p}^*)_{P\&PF}$ and $R_f^*/R_{f,p}^*)_{part}$. The ratio $[R_f^*/R_{f,\,p}^*)_{P\&PF}]/[R_f^*/R_{f,\,p}^*)_{part}]$ is also shown in Table 3. Table 3 shows that the $[R_f^*/R_{f,\,p}^*)_{P\&PF}]/[R_f^*/R_{f,\,p}^*)_{part}]$ ratio is very nearly 1.0 ($1.0 \pm 10\%$). These results suggest that a unique relationship exists between long-term P&PF and accelerated particulate fouling for the present tests. We believe that the observed ratios are significant, in light of the data uncertainty ($\pm 6.2\%$ for the P&PF data, and 11.8% for the particulate fouling data).

Based on the observed empirical relationship between long-term P&PF and accelerated particulate fouling, one may use particulate fouling data to infer the relative behavior of the same tube geometry in long-term P&PF. For example, if an arbitrary "Tube A" has a higher accelerated particulate fouling rate than that of "Tube B" after 15 h, Tube A will have larger P&PF rate than that of Tube B after one cooling season in an actual cooling tower system. Thus, for operation at the same *Re*, the fouling rate has the same qualitative behavior for different enhancement geometry variables in both long-term P&PF and accelerated particulate fouling.

Seven tube geometries were tested here, and all of them show the proposed relationship. Based on the relationship, we can infer the P&PF characteristics in a cooling tower system by using particulate fouling data, which is much easier to obtain. Thus, the enhanced-to-plain tube asymptotic fouling resistance ratios should depend on the ratio of the heat transfer coefficient and surface shear stress, which may be greater or less than unity. Watkinson [14] referenced Kim and Webb [3] to evaluate his proposal. There is no information on the surface shear stress (τ_w) of helically ribbed tubes in the literature. The closest example is for the transverse ribbed tubes studied by Kim and Webb [3]. They showed that surface shear stress (τ_w) decreases with decreasing p/e and decreasing e/D, and the surface shear stress (τ_w) of a smooth tube is larger than that for enhanced tubes.

6.2. Fouling and heat transfer relationship

The mass transfer coefficient (K_m) may be obtained from the heat-mass transfer analogy. The mass transfer coefficient (K_m) is given by

$$\frac{K_m}{u_m} Sc^{2/3} = \frac{h}{\rho u_m c_p} Pr^{2/3} \tag{5}$$

Eq. (5) shows that a high clean tube heat transfer coefficient should result in high mass transfer coefficient. Hence, enhanced heat transfer surfaces (regardless of what kind of enhancement) should result in higher foulant deposition rates than occur with plain surfaces at the same operating velocity.

The key requirement to use the heat-mass transfer

Table 2
Curve-fitted asymptotic fouling resistance and initial fouling rate ($Re = 16{,}000$)

Tube	2	5	3	6	7	8	4	Plain
$R_f^*)_{P\&PF}$E + 4 (m^2 K/W)	2.38	1.81	1.04	0.86	0.79	0.65	0.62	0.32
$R_f^*)_{part}$E + 4 (m^2 K/W)	0.51	0.37	0.23	n/a	n/a	0.14	0.15	0.07
$R_f^*)_{P\&PF}/R_f^*)_{part}$	4.66	4.89	4.52	n/a	n/a	4.64	4.13	4.57
p/e	2.81	3.31	3.50	5.02	7.05	9.77	9.88	n/a

Table 3
Ratio of asymptotic fouling resistances and ratio of heat transfer coefficient of enhanced tubes relative to the plain tube

Tube	2	5	3	6	7	8	4	Plain
$R_f^*/R_{f,p}^*)_{P\&PF}$	7.43	5.65	3.25	2.68	2.46	2.03	1.93	1.0
$R_f^*/R_{f,p}^*)_{part}$	7.28	5.28	3.28	n/a	n/a	2.00	2.17	1.0
$R_f^*/R_{f,p}^*)_{P\&PF}/[R_f^*/R_{f,p}^*)_{part}]$	1.02	1.08	0.99	n/a	n/a	1.02	0.90	
h/h_p	2.32	2.26	2.33	2.08	1.93	1.51	1.74	1.0

analogy is that the mass transport occurs within the diffusion region. For particles of 3.0 μm, the particle transport will be diffusion controlled. In the diffusion regime, particles move with the fluid and are carried to the wall through the viscous sublayer by Brownian motion. The 3.0 μm size particles can be treated as large molecules, and K_m can be predicted via turbulent heat transfer data (or correlations) via the heat–mass transfer analogy.

Watkinson [14] states that most applicable experimental results of scaling on enhanced tubes have involved some particulate deposition. He used the heat-mass transfer analogy to obtain the following equation for crystallization fouling and particulate fouling:

$$\frac{R_f^*}{R_{f,p}^*} = \frac{h/h_p}{\tau_{we}/\tau_{wp}} \tag{6}$$

Table 3 also shows the ratio of the enhanced-to-plain tube heat transfer coefficients (clean tube data). The clean tube data are reported and discussed by Webb et al. [12]. It is interesting to compare the R_f^* ratios (enhanced-to-plain tube) with the h/h_p ratios, which are shown in Fig. 4. The h/h_p ratios vary from 1.51 to 2.33. For $h/h_p < 2.2$, the R_f^* ratio linearly increases with increasing h/h_p. However, for Tubes 2, 3, and 5, which all have very nearly the same h/h_p ($2.26 \le h/h_p \le 2.33$), the linear relationship fails. All three tubes have 35–45° helix angle. Of these three tubes, Tube 2, which has the highest number of starts, smallest p/e and smallest e/D, has the highest R_f^*. Tube 3, has the lowest R_f^* of the three, and has the fewest number of starts (30) and the highest p/e. Since the three tubes have nearly the same h-value, their K_m values are also nearly equal, so the deposition rate would be the same for all three. However, the Kern and Seaton [11] model shows that the $R_f^* \propto K_m/\tau_w$. The surface shear stress (τ_w) is not proportional to pressure drop in helically ribbed tubes, because of pressure drag caused by flow separation. Tubes 2, 3, and 5 all have smaller p/e (resulting in low velocity recirculating zones in the axial zone between ribs), larger helix angle (causing higher pressure drag), and smaller e/D than for the other helically ribbed tubes. Hence, it is probable that they will have smaller τ_w than for the tubes having a smaller number of starts, larger e/D or smaller helix angles. It is probable that the small p/e of Tube 2 causes small τ_w and is responsible for its high R_f^*. Fig. 5 suggests that significant fouling will occur when $p/e < 4.0$.

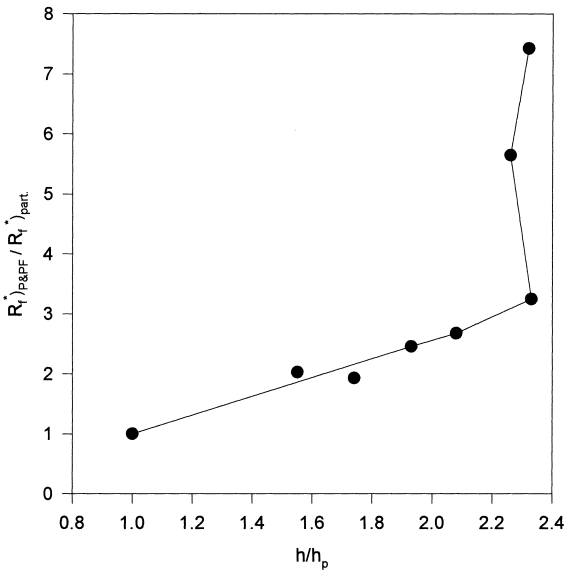

Fig. 4. Fouling ratio (P&PF) versus heat transfer coefficient ratio, referred to plain tube.

Although the deposition rate is proportional to K_m, and $K_m \propto h$, we cannot conclude that high K_m will necessarily result in a high R_f^*. It is also necessary to consider the effect of the enhancement geometry on the foulant removal process. A geometry that provides small wall shear stress in the interfin region will be a candidate for high R_f^*-as is the case for the small p/e, high helix angle tubes.

6.3. Effect of internal surface geometry

In Part I [1], we stated that the dominant parameter affecting fouling in the helical-rib tubes is the p/e geometric variable. Now, we will consider the effect of other geometric variables, for the helical-rib tubes — e/D_i and α (helix angle). The effects of flow patterns on

fouling should be the same for both of particulate fouling and P&PF. The R_f^* values of P&PF shown in Table 2 were correlated using a multiple regression correlation program. The p/e, e/D_i and α were chosen as functional groups. The result is

$$\left(R_f^*\right)_{P\&PF} \propto (p/e)^{-1.2}(e/D_i)^{0.00038}\alpha^{0.00014} \quad (7)$$

Eq. (7) shows that the effects of e/D_i and α on R_f^* are very small, so p/e is confirmed to be the dominant functional group. By correlating R_f^* with p/e in Table 2, we obtained the following correlations, which may be useful in selecting helically ribbed tube geometries:

$$R_f^* = 4.64 \times 10^{-3}(p/e)^{5.72} \quad N \leq 25$$

$$R_f^* = 1.85 \times 10^{-4}(p/e)^{0.92} \quad N > 25 \quad (8)$$

Fig. 5 shows the two correlations.

7. Conclusions

1. Accelerated particulate fouling and long-term P&PF fouling show a unique relationship, both for plain and enhanced tubes. This allows one to infer the relative long-term P&PF performance of different enhanced tube geometries from accelerated particulate fouling data.
2. For a small number of ridge starts (less than 25) and helix angles below 35°, the fouling potential is proportional to the heat transfer coefficient (or the mass transfer coefficient, via the heat-mass transfer analogy). However, for a large number of starts and high helix angles (e.g., 45°), the fouling factor is considerably higher than one would predict based on the mass transfer coefficient. It appears that this occurs because of low shear stress (affecting the foulant removal rate) in the interfin region.
3. Design correlations are provided that will allow the engineer to determine the effect of p/e on P&PF fouling.

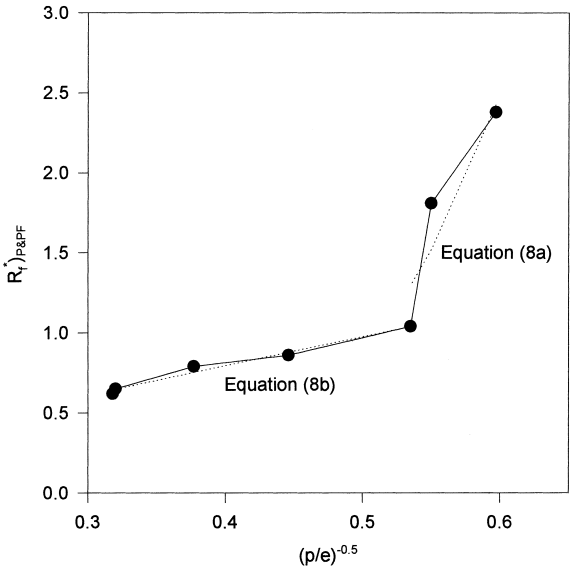

Fig. 5. The relationship between fouling resistance and p/e.

Acknowledgements

This project was principally funded by EPRI, with additional financial support from The Trane Co., Carrier Corp., and Wolverine Tube Corp. See complete Acknowledgment in Webb and Li [1].

References

[1] R.L. Webb, W. Li, Fouling in enhanced tubes using cooling tower water Part I: long term fouling data, International Journal of Heat and Mass Transfer 43 (2000) 3567–3578.
[2] T.J. Rabas, et al., Comparison of power-plant condenser cooling-water fouling rates for spirally-indented and plain tubes, Heat Transfer Engineering 14 (4) (1993) 58.
[3] N-H. Kim, R.L. Webb, Particulate fouling of water in tubes having a two-dimensional roughness geometry, International Journal of Heat and Mass Transfer 34 (11) (1991) 2727.
[4] L.M. Chamra, R.L. Webb, Modeling liquid-side particulate fouling in enhanced tubes, International Journal of Heat and Mass Transfer 37 (4) (1994) 571.
[5] E.F.C. Somerscales, A.F. Ponteduro, A.E. Bergles, Particulate fouling of heat transfer tubes enhanced on their inner surface, Fouling and Enhancement Interactions HTD-164 (1991) 17.
[6] J. Taborek, J.G. Knudsen, T. Aoki, R.B. Ritter, J.W. Palen, Fouling the major unresolved problem in heat transfer, Part I: fouling mechanisms, their characteristics and factors influencing them, Chemical Engineering Progress V-88 (2) (1972) 59–67; (7) 67–78.
[7] N. Epstein, Fouling in heat exchangers, in: Proceedings of the Sixth International Heat Transfer Conference, 6, 1979, pp. 235–253.
[8] S.G. Yiantsios, A.J. Karabelas, Detachment of spherical micro particles adhering on flat surfaces by hydrodynamic forces, Journal of Colloid Interface Science 176 (1995) 74–85.
[9] D. Hasson, Progress in precipitation fouling research — a review, in: Proceedings of Fouling Mitigation of Industrial Heat-Exchange Equipment, An International Conference, 1997.
[10] B. Bansal, H. Muller-Steinhagen, X.D. Chen, Effect of

suspended particles on crystallization fouling in plate heat exchangers, Journal of Heat Transfer 119 (1997) 568–574.
[11] D.Q. Kern, R.A. Seaton, A theoretical analysis of thermal surface fouling, British Chem. Eng. (4) (1959) 258–262.
[12] R.L. Webb, R. Narayanamurthy, P. Thors, Heat transfer and friction characteristics of internal helical-rib roughness, Journal of Heat Transfer 122 (2000) 122–134.
[13] Wei Li, A theoretical and experimental study of fouling in enhanced tubes in cooling tower systems, Ph.D. Thesis, Penn State University, 1998.
[14] A.P. Watkinson, Interactions of enhancement and fouling, Fouling and Enhancement Interactions HTD-164 (1991) 1.